Hindawi
International Journal of Photoenergy
Volume 2021, Article ID 7506837, 13 pages
https://doi.org/10.1155/2021/7506837

Research Article

Numerical Design of Ultrathin Hydrogenated Amorphous Silicon-Based Solar Cell

F. X. Abomo Abega, A. Teyou Ngoupo, and J. M. B. Ndjaka

Université de Yaoundé 1, Faculté des Sciences, Département de Physique, BP, 812 Yaoundé, Cameroon

Correspondence should be addressed to A. Teyou Ngoupo; arielteyou@yahoo.fr

Received 1 June 2021; Revised 14 July 2021; Accepted 2 August 2021; Published 14 August 2021

Academic Editor: Kok Keong Chong

Numerical modelling is used to confirm experimental and theoretical work. The aim of this work is to present how to simulate ultrathin hydrogenated amorphous silicon- (a-Si:H-) based solar cells with a ITO BRL in their architectures. The results obtained in this study come from SCAPS-1D software. In the first step, the comparison between the J-V characteristics of simulation and experiment of the ultrathin a-Si:H-based solar cell is in agreement. Secondly, to explore the impact of certain properties of the solar cell, investigations focus on the study of the influence of the intrinsic layer and the buffer layer/absorber interface on the electrical parameters (J_{SC}, V_{OC}, FF, and η). The increase of the intrinsic layer thickness improves performance, while the bulk defect density of the intrinsic layer and the surface defect density of the buffer layer/*i*-(a-Si:H) interface, respectively, in the ranges [$10^9\,cm^{-3}$, $10^{15}\,cm^{-3}$] and [$10^{10}\,cm^{-2}$, $5\times10^{13}\,cm^{-2}$], do not affect the performance of the ultrathin a-Si:H-based solar cell. Analysis also shows that with approximately 1 μm thickness of the intrinsic layer, the optimum conversion efficiency is 12.71% ($J_{SC} = 18.95\,mA\cdot cm^{-2}$, $V_{OC} = 0.973\,V$, and FF = 68.95%). This work presents a contribution to improving the performance of a-Si-based solar cells.

1. Introduction

The photovoltaic industry is over 95% focused on the use of silicon as a base material [1]. The cost of synthesizing this material has made it possible to switch from crystalline silicon (c-Si) to amorphous silicon (a-Si). Thin-film silicon, mainly the amorphous silicon (a-Si:H) solar cells, has the potential to be less expensive due to low material consumption, lower thermal budget manufacturing steps, and low temperature coefficient of solar cell efficiency [2]. However, the commercially available stabilized efficiency and reliability of a-Si:H solar cells are greater than many of the third generation solar cells as reported so far [3]. When synthesizing amorphous silicon, it has a high concentration of dangling bonds in its structure. To overcome this failure, it is necessary to incorporate hydrogen [4]. This defect reduction allowed the doping of hydrogenated amorphous silicon with boron and phosphorus [5]. The a-Si:H has the advantage of having an adjustable bandgap and a high optical absorption coefficient. This optical bandgap varies between 1.6 eV and 1.8 eV [6]. The efficiency limit for a single bandgap thin film-based solar cell predicted by Shockley and Queisser is around 31% [7]. Nowadays, the maximum conversion efficiency of a-Si:H solar cells is 10.2% [8], which is still far from the theoretical value. There are several methods of manufacturing a-Si:H-based solar cells such as photo PECVD [9], sputtering [10]. The most suitable for manufacturing single-junction solar cells is the PECVD process [11]. However, some limits should be placed on the preeminence of a-Si:H-based solar cells, since a degradation effect caused by exposure to light was highlighted by the Staebler-Wronski effect [12]. Indeed, they observed that exposure to the light of an a-Si:H-based solar cell, stretched over time, caused a drop of its electrical parameters: this is known as a light-induced degradation (LID) effect. This limitation can be reduced by controlling the thickness of the intrinsic (*i*) layer in the structure of solar cell [13, 14]. In the a-Si:H-

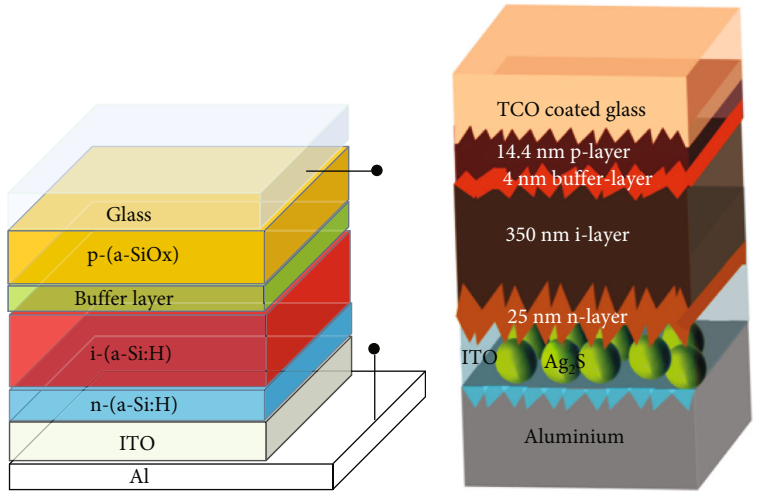

(a) Cell to be simulated (b) Experimental structure

Figure 1: Schematic diagram of solar cells.

based solar cell, the thickness of the *i*-layer controls the short-circuit current [3].

To facilitate light absorption in a-Si:H-based solar cell, some advanced tricks are required to utilize the major portion of the incident light in the active layer of the cell, like light-trapping techniques in order to enhance the optical path length (OPL) of photons [3]. The optical absorption and carrier collection can be increased by improving the reflection characteristics of a back reflector layer (BRL). There are multiple approaches to suppress the optical losses in the device; hence, properly designing the device is crucial [3]. This work presented how to use numerical simulation in the case of a-Si:H-based solar cell with a nonconventional back reflector layer (BRL) in their structures. A nonconventional BRL is definite as BRL containing semiconductor nanoparticles. This type of BRL improves the reflection characteristics of a back reflector layer. Nonconventional BRL contributes in reducing optical losses by light scattering behaviour, improves absorbance, and ameliorates photon management. In this approach, this can be numerically modelled through the rate of reflection at the rear contact and the absorption coefficient of the active layer (*i*) of the a-Si:H-based solar cell in the SCAPS-1D software. As is known to all, the device quality is mainly determined by factors including emitter quality and interface quality [15]. In order to validate our solar cell model, we start from a comparative study of the J-V characteristic of the results of the experiment and simulation, and on the other hand, we study the influence of the various parameters (thickness, bulk defects density, and properties of buffer layer/absorber interface) on the performance of the solar cell, using SCAPS-1D software.

2. Method and Materials

2.1. Method. Numerical modelling is an approach and an important tool which allows to understand the complexity of solar cells and the development of these; it also helps to understand the phenomena that are at the origin of the limitation of the conversion efficiency of solar cells. SCAPS-1D is a one-dimensional numerical simulation software of solar cells [16]; it was developed at the University of Gent in Belgium and was previously tested on the structures of CuInSe2 and CdTe family [17]. But with the evolution of research, its functions have extended to crystalline (Si, GaAs) and amorphous (a-Si, micromorphic Si) structures. Thus, his choice is justified in this work by the fact that it allows to have simulation results in agreement with experience [16].

The descriptive equations used by SCAPS-1D software are the basic semiconductor equations (equations (1)–(3)). They are three coupled and nonlinear differential equations that are solved simultaneously in SCAPS-1D.

$$\frac{\partial}{\partial x}\left(\varepsilon_0\varepsilon\frac{\partial\psi}{\partial x}\right) = -q\left(p - n + N_D^+ - N_A^- + \frac{\rho_{\text{def}}}{q}\right), \quad (1)$$

$$\frac{\partial J_n}{\partial x} - U_n + G = \frac{\partial n}{\partial t}, \quad (2)$$

$$\frac{\partial J_p}{\partial x} - U_p + G = \frac{\partial p}{\partial t}. \quad (3)$$

Equation (1) is called the Poisson equation; it describes the phenomena of an electrostatic nature, where ψ is the electrostatic potential, n and p are the density of free electrons and holes, respectively, N_D^+ and N_A^- are the concentrations of ionized donors and acceptors, respectively, and ρ_{def} is the density of deep defect centers. Equations (2) and (3) are the continuity equations of electrons and holes; they govern the condition of dynamic equilibrium in a semiconductor; G is the generation rate; U_n and U_p are the recombination rates of electrons and holes, respectively. J_n and J_p represent the current densities of electrons and holes, respectively; and their expressions are given, respectively, by equations (4) and (5), where μ_n is the electron mobility and μ_p the hole

Table 1: Input parameters in SCAPS-1D.

Parameters	p-(a-SiO$_x$)	Buffer layer	i-(a-Si:H)	n-(a-Si:H)	ITO
Thickness (μm)	0.500	0.004	0.350	0.025	0.060
Bandgap energy (eV)	1.950	1.800	1.800	1.800	3.650
Electron affinity (eV)	4.000	3.900	3.900	3.900	4.800
Dielectric permittivity (relative)	9.000	11.900	11.900	11.900	8.900
CB effective density of states (cm^{-3})	2.20×10^{18}	1.0×10^{20}	1.0×10^{20}	1.0×10^{20}	5.2×10^{18}
VB effective density of states (cm^{-3})	1.80×10^{19}	1.0×10^{20}	1.0×10^{20}	1.0×10^{20}	1.0×10^{18}
Electron thermal velocity (cm/s)	10^7	10^6	10^6	10^7	2.0×10^7
Hole thermal velocity (cm/s)	10^7	10^6	10^6	10^7	2.0×10^7
Electron mobility (cm^2/Vs)	5.0	50	20	30	50
Hole mobility (cm^2/Vs)	1.0	10	5.0	5.0	25
Donor density N_D (cm^{-3})	0.0	0.0	1.0×10^6	1.0×10^{18}	1.0×10^{20}
Acceptor density N_A (cm^{-3})	1.0×10^{17}	7.0×10^{15}	1.0×10^6	0.0	0.0
Absorption coefficient	SCAPS	SCAPS	SCAPS	SCAPS	SCAPS

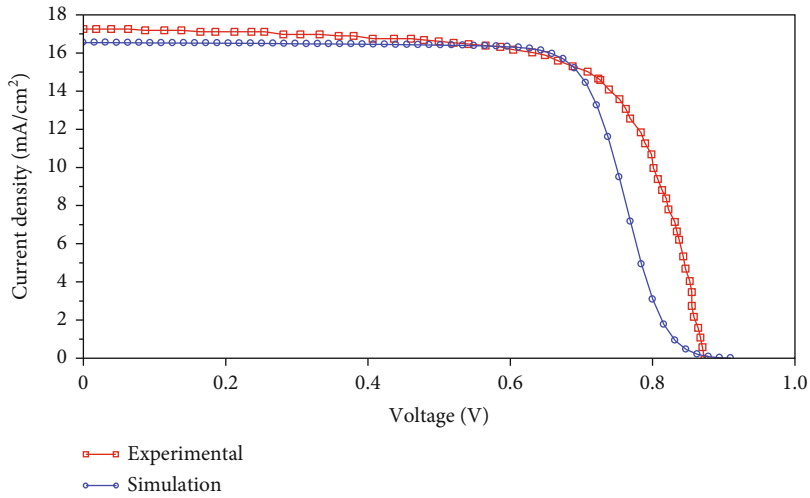

Figure 2: Experimental and simulated J-V characteristics of the a-Si:H-based solar cell.

mobility; E_{Fn} is the Fermi level of electrons, and E_{Fp} the Fermi level of holes.

$$J_n = -\frac{\mu_{n^n}}{q}\frac{\partial E_{Fn}}{\partial x}, \quad (4)$$

$$J_n = -\frac{\mu_{p^p}}{q}\frac{\partial E_{Fp}}{\partial x}. \quad (5)$$

2.2. Materials. Generally, the performance of solar cells is dependent on three main factors: material selection, material growth technique, and device architecture [18]. A solar cell consists of a semiconductor material that absorbs light and then generates excess electrons and holes [15]. Figure 1 is the structure of a-Si:H-based solar cells. Figure 1(a) shows the structure of the solar cell investigated in this work, while Figure 1(b) represents the schematic diagram of the solar cell

Table 2: Experimental and simulated electrical parameters of the a-Si:H-based solar cell.

Parameters	Experimental	Simulation
J_{SC} (mA·cm^{-2})	17.2	16.55
V_{OC} (V)	0.87	0.905
FF (%)	70.0	70.62
η (%)	10.58	10.58

from the experimental work of Banerjee et al. [3]. In this subsection, we describe the structure of the solar cell to be optimized. This single-junction cell (Figure 1(a)) is based on hydrogenated amorphous silicon and is constructed using SCAPS-1D software. The improvement of its electrical parameters depends on the different properties and the arrangement of the layers in the structure. Cell to be

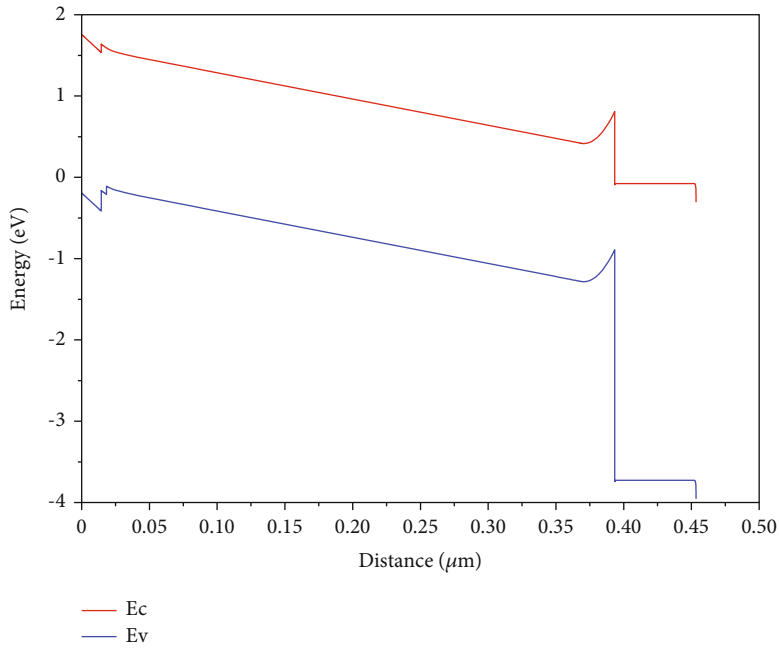

Figure 3: Energy band diagram of p-(a-SiO$_x$)/buffer layer/i-(a-Si:H)/n-(a-Si:H)/ITO/Al solar cell.

simulated is structured as follows: p-(a-SiO$_x$)/buffer layer/i-(a-Si:H)/n-(a-Si:H)/ITO/Al, as shown in Figure 1(a).

The i-(a-Si:H) layer, intrinsic type, is situated between the p-doped buffer layer and the n-doped n-(a-Si:H) layer; it is the fundamental element of the solar cell in which the photovoltaic conversion takes place. This layer is called an absorber layer. The light enters the structure through the p-(a-SiO$_x$) window layer, its bandgap depends on the O/Si ratio, and when this ratio is 34%, it has an intermediate bandgap of 1.95 eV, with a conductivity of 3.3 S/cm [19]. This layer maximizes the absorption of light in the structure. The photons absorbed by the i-layer create the electron-hole pairs. The induced electric field, by the n- and p-layers through the i-layer, causes the electrons to drift towards the n region and the holes towards the p region. The p-type-doped buffer layer reduces the height of the Schottky barrier and the recombination at the p-(a-SiO$_x$)/i-(a-Si:H) interface [20]. The ITO layer is an important layer in this numerical simulation; it can increase the optical absorption and carrier collection by improving the reflection characteristics of a back reflector layer (BRL, which is a layer between the metal back contact and the bottom n-layer in a-Si:H solar cell) [3]. The ITO layer also reduces transmission losses at the rear contact (Al metallic contact) and promotes adhesion between the amorphous silicon and the metallic contact [21]. Improving the photovoltaic conversion efficiency requires improving the utilization of the major portion of the solar spectrum in the active layer, in order to enhance the OPL of photons [3]. In this work, we are trying to understand how the presence of ITO BRL in a-Si:H solar cell contributes to enhance its performances with SCAPS-1D software.

To model this type of amorphous silicon solar cell structure, taking into account the effect of ITO BRL containing semiconductor nanoparticles which ameliorates photon management and increases the generation of electron-hole pairs, in the environment of SCAPS-1D, the optical absorption submodel applied at the i-layer is based on the square-law model, given by equation (6). The value of the absorption coefficient represents how efficiently the photon energy will be harvested using the materials [7]. BRL plays a crucial role in light reflection by backscattering to the active layer of the cell; thus, the reflection rate at the rear contact is taken at more than 93% in this numerical simulation as suggested by the experimental work of Banerjee et al. [3].

$$\alpha(\lambda) = \left(A + \frac{B}{h\nu}\right)\sqrt{h\nu - E_g}, \tag{6}$$

where E_g represents the gap, and A (cm^{-1}·eV$^{-1/2}$) and B (cm^{-1}·eV$^{+1/2}$) are the parameters of the model in SCAPS-1D.

The electrical input parameters of all materials used in this numerical simulation, for the resolution of the previous equations, are given in Table 1; these data are taken from the literature [3, 19, 22, 23]. In this simulation study, metal contacts (front and back contacts) are assumed to be flat bands.

3. Results and Discussion

3.1. Comparison between Simulation and Experience. First, we validate our solar cell structure model (Figure 1(a)), by comparing the experimental results of the current-voltage characteristic from the work of Banerjee et al. [3] to those of the numerical simulation as shown in Figure 2. The modelling of the a-Si:H-based solar cell (Figure 1(a)) is made under AM1.5 solar spectrum, a light power of 1000 W/m^2, and at 300 K, using the parameters of Table 1. In this numerical simulation model, the silver sulfide nanomirrors in ITO

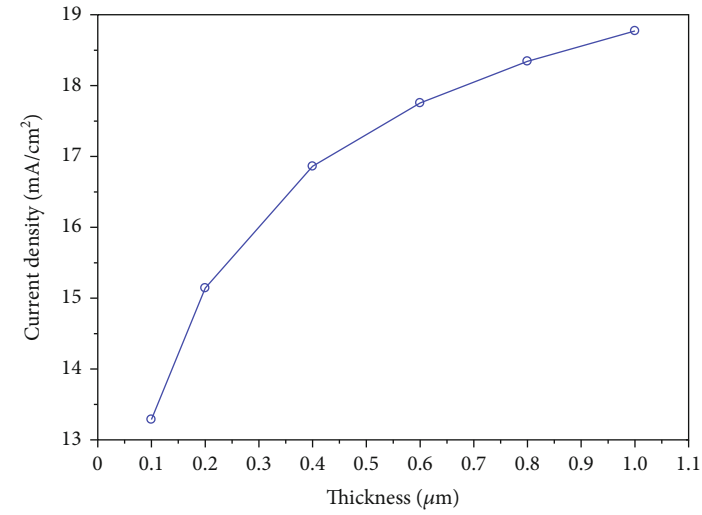

(a)

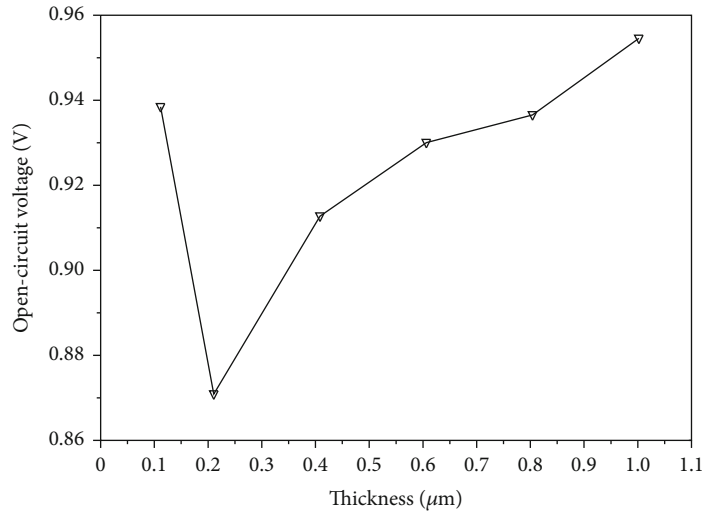

(b)

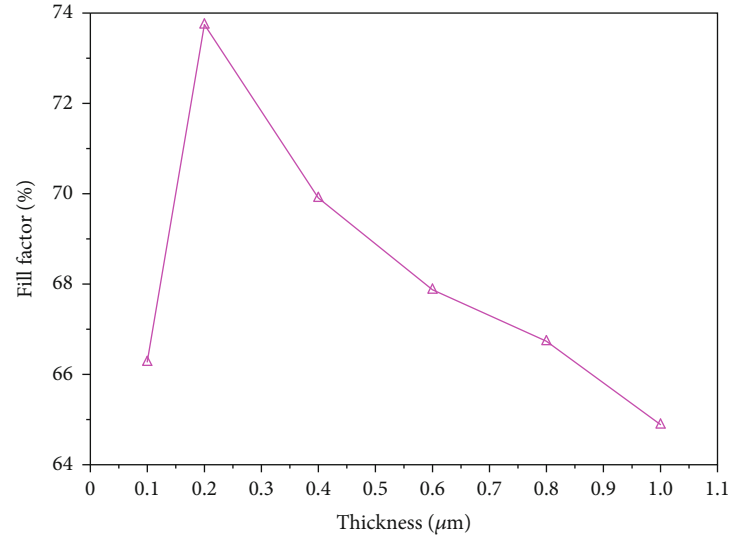

(c)

Figure 4: Continued.

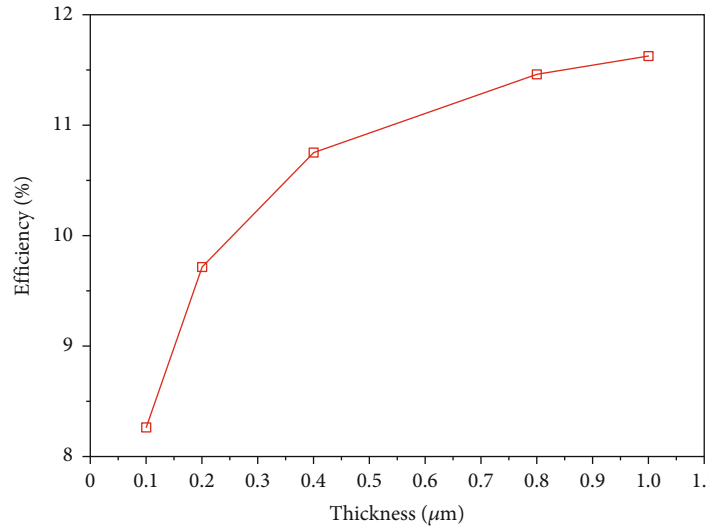

Figure 4: Influence of the variation of the intrinsic layer *i*-(a-Si:H) thickness on the electrical parameters: (a) J_{SC}, (b) V_{OC}, (c) FF, and (d) η.

BRL (nonconventional BRL) of the experimental model were taken into account, assuming a reflection of the order of 95% at the rear contact of the a-Si:H-based solar cell and the absorption coefficient given by equation (6) for the *i*-layer of the solar cell.

Further, the short-current density (J_{SC}), fill factor (FF), open-circuit voltage (V_{OC}), and conversion efficiency from experiment and simulation are illustrated in Table 2. In view of the data from Table 2, we can therefore conclude that there is a good agreement between the experimental and simulation results; this confirms the validity of the a-Si:H-based solar cell model (Figure 1(a)). Figure 3 represents the band diagram of this simulated cell at thermal equilibrium.

3.2. Influence of the Intrinsic Layer Thickness Variation. The main drawback of a-Si:H solar cells is light-induced degradation (LID), which can be minimized by controlling the thickness of the intrinsic (*i*) layer [3]. It is useful to be able to appreciate the importance of studying the variation of thickness of the intrinsic layer on the performance of a-Si:H-based solar cell, because it is in this layer that happens the phenomenon of photovoltaic conversion, resulting in the production of photovoltaic energy. Thus, this subsection allows us to investigate the effect of the variation of the thickness of the intrinsic layer on the electrical parameters of the solar cell, as shown in Figure 4. For this study, the thickness of the intrinsic layer varies from 0.1 μm to 1 μm in the case of solar cells with ultrathin absorber layer, by keeping constant the other parameters of the layers of the structure of solar cell (Figure 1(a)) and by neglecting the properties of interfaces between the different layers. Within this variation range of the intrinsic layer thickness, we observe an increase in the short-circuit current density from 13.28 mA·cm^{-2} to 18.75 mA·cm^{-2} (Figure 4(a)). Therefore, the short-circuit current density increases with the thickness. This result is explained by the considerable absorption of incident photons in the intrinsic layer, which increases the number of photogenerated carriers [6], through the generation rate as shown in equation (7). Similarly, the work of Chelvanathan et al. [24] has shown that the current density also increases with thickness in the case of the CIGS-based solar cell.

$$J_{ph} = q \bullet G \bullet \left(L_n + W + L_p\right), \tag{7}$$

where L_n and L_p are the diffusion lengths of electrons and holes, respectively, and W is the width of the space charge region.

The open-circuit voltage V_{OC} (Figure 4(b)) increases as the thickness of the intrinsic layer increases in the range [0.2 μm, 1 μm]; this can be attributed to a decrease in the phenomenon of bulk recombination and at the level of back contact, and better passivation of the *i*-(a-Si:H)/*n*-(a-Si:H) interface as suggested by Lachaume [25] and De Wolf et al. [26] in their works. The increase of the open-circuit voltage thus reflects the nondegradation of the *i*-(a-Si:H)/*n*-(a-Si:H) junction. On the other hand, the decrease in V_{OC} in the range [0.1 μm, 0.2 μm] can be attributed to the degradation of the *i*-(a-Si:H)/*n*-(a-Si:H) junction and to the recombination phenomenon at the interface of this junction.

In addition, the fill factor FF (Figure 4(c)) also shows two trends: a first in the range [0.1 μm, 0.2 μm] and a second in the range [0.2 μm, 1 μm]. The increase in FF in the interval [0.1 μm, 0.2 μm] may be due to the reduction in the double diode effect observed in the *i*-(a-Si:H) layer [27]. However, the decrease in FF in the interval [0.2 μm, 1 μm] is due to the presence of coordination defects in the absorber layer, and secondly, the resistance of the intrinsic layer increases with its thickness, which increases series resistance of the solar cell.

In view of the above, the combined action of these three parameters (J_{SC}, V_{OC}, and FF) contribute to an increase of conversion efficiency (equation (8)) of the a-Si:H-based solar

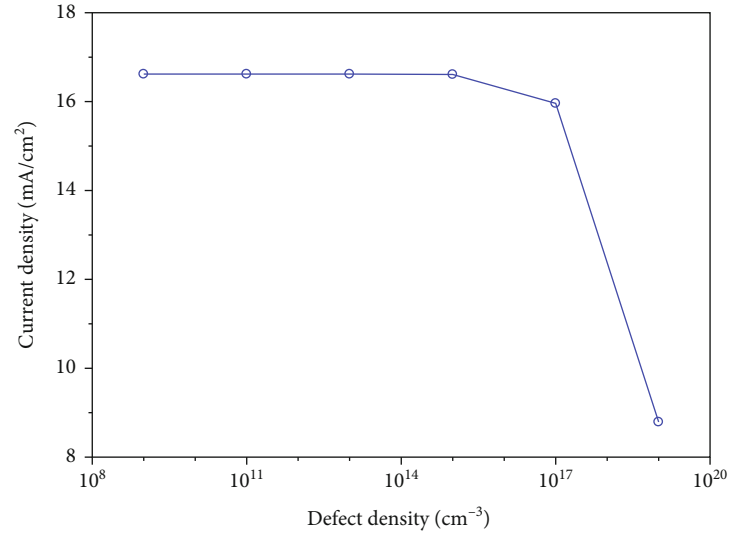

(a)

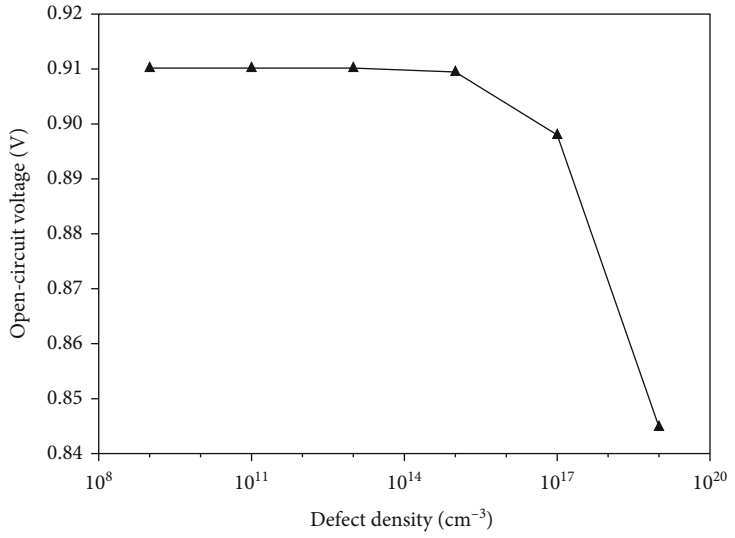

(b)

Figure 5: Continued.

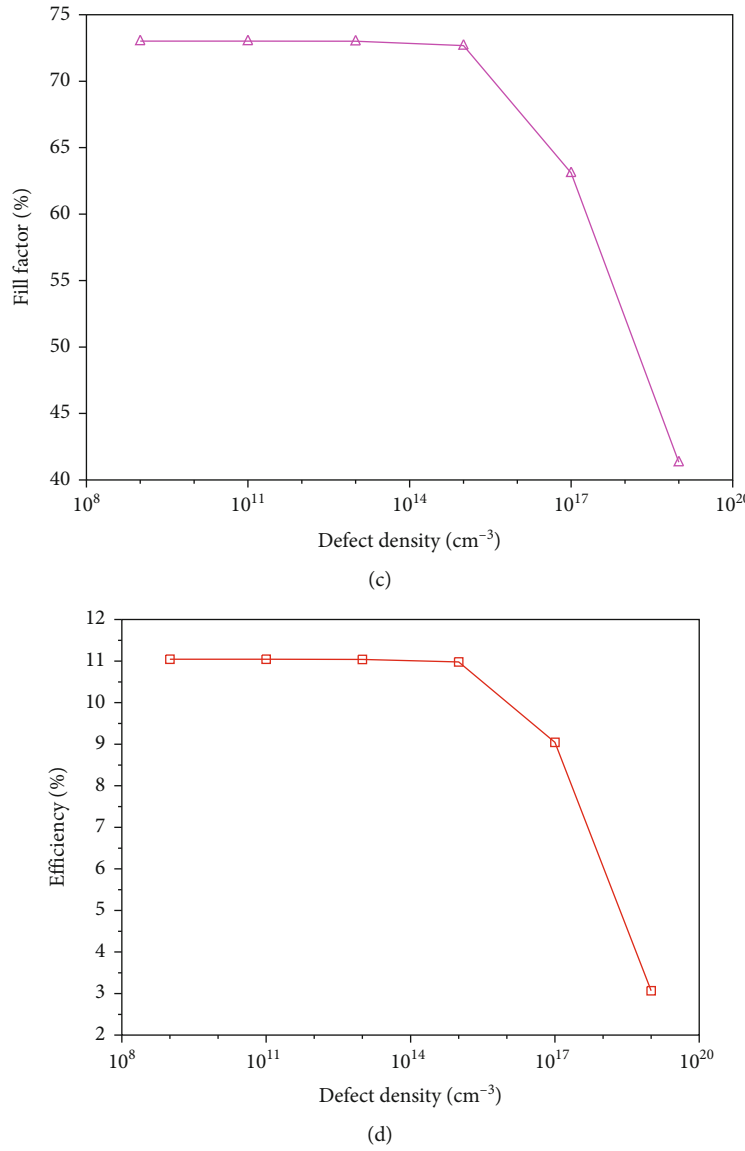

Figure 5: Influence of the variation of the bulk defect density of the intrinsic layer *i*-(a-Si:H) on the electrical parameters: (a) J_{SC}, (b) V_{OC}, (c) FF, and (d) η.

cell, as a function of the thickness of the intrinsic layer (Figure 4(d)); therefore, we observe a variation of the conversion efficiency from 8.26% to 11.63%.

$$\eta = \frac{J_{SC} \bullet V_{OC} \bullet FF}{P}. \quad (8)$$

3.3. Influence of the Defect Density in the Intrinsic Layer. Figure 5 shows the effect of varying deep bulk defect density (N_t), acceptor type, of the intrinsic layer on the performance parameters of the a-Si:H-based solar cell using the data from Table 1 and for N_t ranging from $10^9\,cm^{-3}$ to $10^{19}\,cm^{-3}$. These defects form following the breakdown of the chemical equilibrium of the weak Si-Si bonds during the deposition of amorphous silicon [28]. Their energy distribution in the bandgap varies depending on the incorporation of the proportions of hydrogen in the intrinsic layer; by convention, these defects are located in the upper part of the bandgap. The results obtained show that, for N_t took in the range [$10^9\,cm^{-3}$, $10^{15}\,cm^{-3}$], the electrical parameters (J_{SC}, V_{OC}, FF, and η) are constant (Figure 5). In this region, the donor density ($10^6\,cm^{-3}$) is the same as acceptors. Taking into account the amorphous nature, the intrinsic layer can be considered to be heavily doped; therefore, the combined effects

Table 3: Properties of buffer layer/absorber layer interface.

Parameters	Buffer layer/*i*-(a-Si:H)
D_{it} (cm^{-2})	Variable (A)
σ_n (cm^2)	10^{-15}
σ_p (cm^2)	10^{-15}

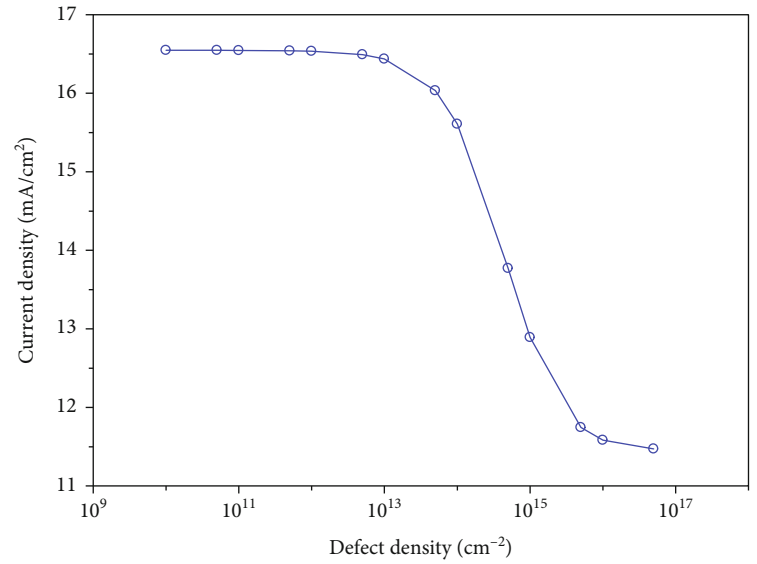

(a)

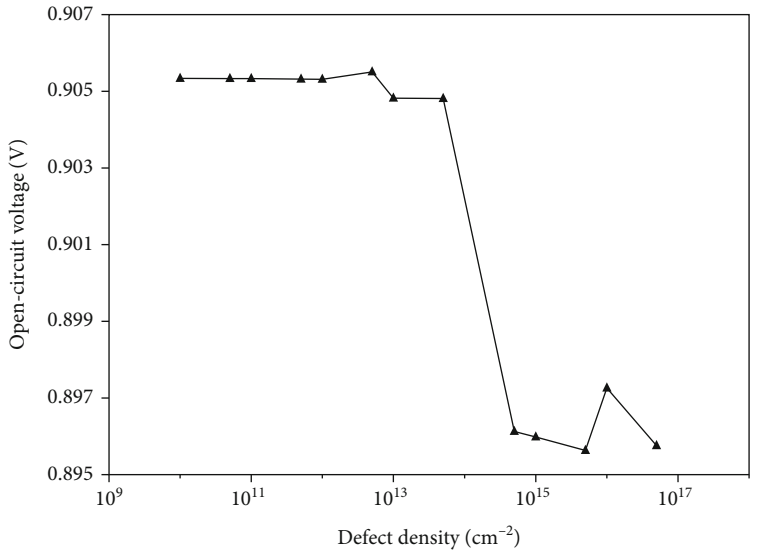

(b)

Figure 6: Continued.

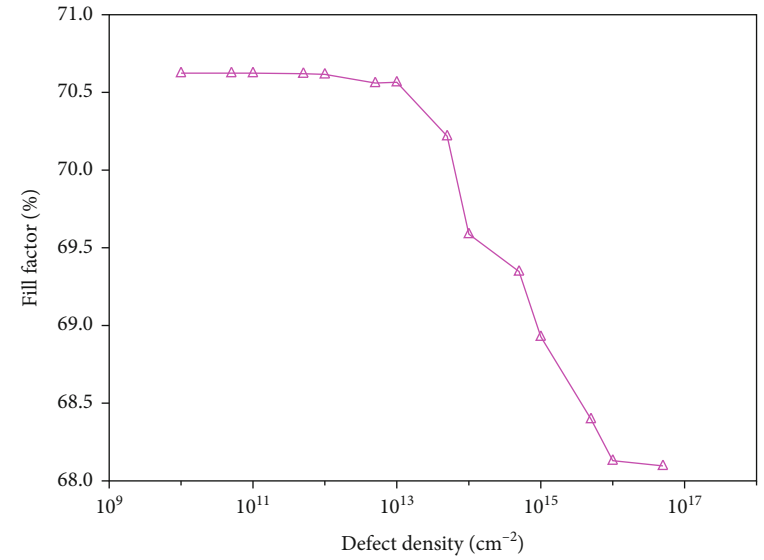

(c)

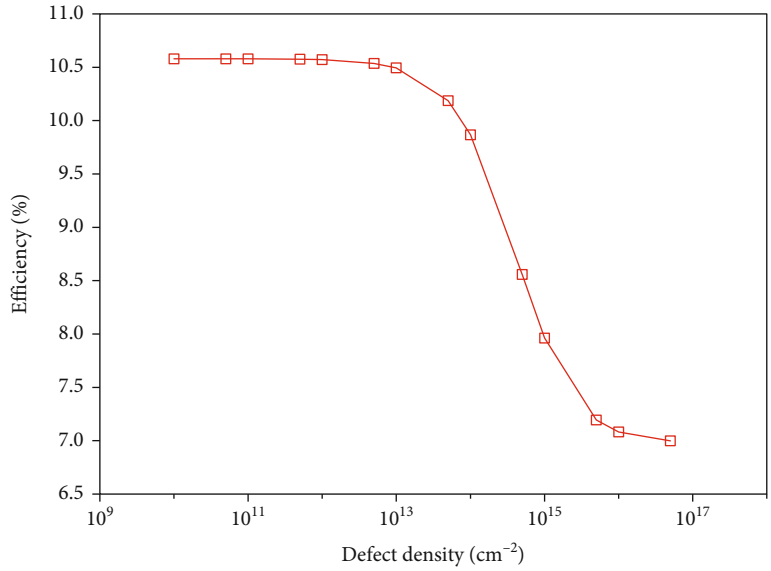

(d)

Figure 6: Effect of varying buffer layer/*i*-(a-Si:H) interface states on electrical parameters: (a) J_{SC}, (b) V_{OC}, (c) FF, and (d) η.

of acceptors and donors compensate that of bulk defects. In other words, the recombination rate is negligible in the intrinsic layer.

On the other hand, we observe that, for N_t took in the range [10^{15} cm^{-3}, 10^{19} cm^{-3}], all the electrical parameters are greatly affected by the variation of the bulk defect density; there is an abrupt decrease of all these parameters (Figure 5). This decrease is reflected in the fact that the increase of these defects creates localized states in the band-gap [29, 30]. These localized states influence the intrinsic Fermi level by creating tail states and by inducing additional charges, which are taken into account in the ρ_{def} term of equation (1). Thus, the phenomena of recombination of the photogenerated carriers in this layer predominate over the phenomena of generations. The current density J_{SC} decreases from 16.61 mA/cm^2 to 8.79 mA/cm^2, the open-circuit voltage V_{OC} from 0.910 V to 0.845 V, the fill factor FF from 73.0% to 41.33%, and the efficiency from 11.04% to 3.07%. The presence of these defects is the cause of optical loss due to a high Shockley-Read-Hall recombination rate, resulting in a sharp decline in all electrical parameters. These results are in agreement with those of the work of Ghahremani and Fathy [31].

3.4. Effect of State Density of Buffer Layer/Absorber Interface. Defect states at the interface of two layers can cause strong interface recombination in solar cell. A low interface state in the midgap can be achieved by the insertion of intrinsic hydrogenated amorphous silicon in the a-Si/c-Si passivated contact (a-PC) solar cell [15]. Modelling and optimizing a solar cell require controlling the interface states between the

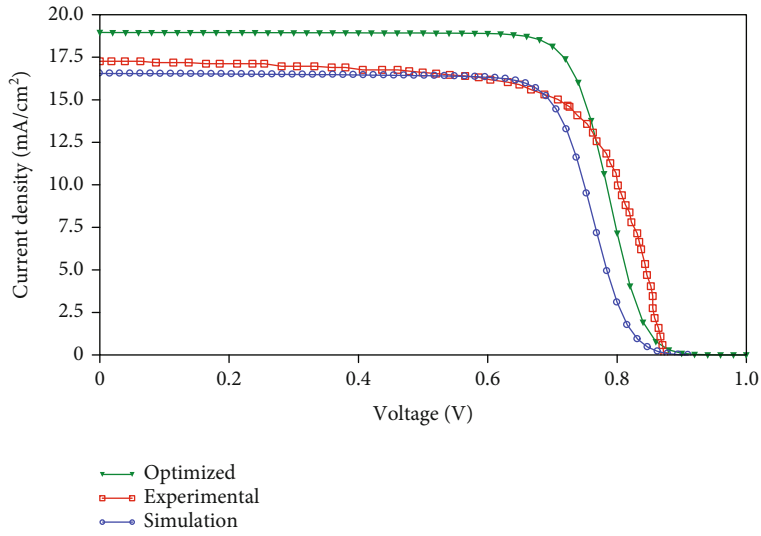

Figure 7: Experimental, simulated, and optimized J-V characteristics of the a-Si:H solar cell.

different layers that constitute it, in order to ensure the passage of charge carriers through a junction. The previous results are obtained by neglecting the interface properties between the different layers. The buffer layer/absorber interface plays a crucial role in the charge transport mechanism in a-Si:H solar cells [32]. In this section, we explore the influence of the density of surface defects D_{it} (Table 3) at the buffer layer/*i*-(a-Si:H) interface, using the data from Table 1 and for $N_t = 10^{16}\,\text{cm}^{-3}$ in the intrinsic layer, on the electrical parameters (J_{SC}, V_{OC}, FF, and η) of the a-Si:H-based solar cell, as presented in Figure 6. This density of surface defects (D_{it}) varies from $10^{10}\,\text{cm}^{-2}$ to $5 \times 10^{16}\,\text{cm}^{-2}$.

For surface defect densities ranging from $10^{10}\,\text{cm}^{-2}$ to $10^{13}\,\text{cm}^{-2}$, the electrical parameters are almost insensitive. Moreover, when the density of the surface defects increases from $10^{13}\,\text{cm}^{-2}$ to $5 \times 10^{16}\,\text{cm}^{-2}$, the short-circuit current density decreases drastically from $16.43\,\text{mA/cm}^2$ to $11.47\,\text{mA/cm}^2$ (Figure 6(a)). This decrease is due to increased recombination centers at the interface buffer layer/*i*-(a-Si:H), favouring electron traps but also the loss by optical absorption of the incident light [33].

Figure 6(b) shows that, for D_{it} took in the range $[10^{14}\,\text{cm}^{-2},\ 5 \times 10^{15}\,\text{cm}^{-2}]$, the open-circuit voltage decreases considerably from 0.908 V to 0.896 V. This decrease is the consequence of dangling bonds in the absorber layer, which cause recombination phenomena, and atomic interdiffusion of the buffer layer/*i*-(a-Si:H) interface.

Figure 6(c) shows the variation of the fill factor as a function of the density of the surface defects. For surface defect densities greater than $10^{13}\,\text{cm}^{-2}$, the fill factor decreases from 70.56% to 68.09%. FF is affected by surface recombination at the buffer layer/*i*-(a-Si:H) interface. This decrease can also be explained by an empirical expression of FF as a function of V_{OC} (equation (9)) [32, 34].

$$\text{FF} = \frac{\nu_{oc} - \ln(\nu_{oc} + 0.72)}{1 + \nu_{oc}}, \text{ where } \nu_{oc} = \frac{qV_{OC}}{AkT}. \quad (9)$$

Table 4: Comparison of the electrical parameters of the experimental and optimized solar cell structures.

Parameters	Experimental	Optimized
J_{SC} (mA·cm^{-2})	17.2	18.95
V_{OC} (V)	0.87	0.973
FF (%)	70.0	68.86
η (%)	10.58	12.71

These three electrical parameters (J_{SC}, V_{OC}, and FF) contribute to the decrease of the conversion efficiency (Figure 6(d)) given by equation (8); these results are in agreement with the works of Rached and Rahal [35]. The trend of the influence of interface state density on cell performance is similar to that obtained in the work of Zhou et al. [36].

3.5. Optimized a-Si:H Solar Cell. Optimizing a solar cell consists of finding the values of the parameters that make it the most efficient. In this paper, it is to determine the optimal electrical parameters of our model ultrathin film hydrogenated amorphous silicon solar cell. Our approach in this subsection consists in using the optimal values of the parameters studied in the previous subsections, in order to simulate the electrical parameters of the optimized solar cell. The optimal parameters, previously determined, are $1\,\mu\text{m}$, $10^9\,\text{cm}^{-3}$, and $10^{10}\,\text{cm}^{-2}$, respectively, of the thickness and the bulk defect density of the intrinsic layer and of the density of surface defects of the buffer layer/*i*-(a-Si:H) interface. The optimized cell thus leads to a conversion efficiency of 12.71%. Figure 7 gives the current-voltage characteristics of the three structures used in our work, and Table 4 summarizes the electrical parameters of experimental and optimized solar cells. The decrease in FF from the experimental solar cell to the optimized one is due to the phenomenon of surface recombination at the buffer layer/*i*-(a-Si:H) interface and to the increase in the series resistance of the solar cell, which increases with the thickness of the intrinsic layer.

4. Conclusion

In this work, we present the factors that can be at the origin of the electrical losses in the ultrathin a-Si:H-based solar cell with a ITO BRL, through a study by numerical simulations using the SCAPS-1D software. From the p-(a-SiO_x)/buffer layer/i-(a-Si:H)/n-(a-Si:H)/ITO/Al structure of the solar cell, we simulated the current-voltage characteristic whose electrical parameters ($J_{SC} = 16.55\,mA{\cdot}cm^{-2}$, $V_{OC} = 0.905\,V$, FF = 70.62%, and $\eta = 10.58\%$) reproduce the experimental data, and we have shown how the thickness and bulk defects of the absorber and the density of the surface defects of the buffer layer/i-(a-Si:H) interface affect the electrical parameters of the ultrathin a-Si:H-based solar cell. These properties are crucial for high-performance solar cells. Increasing the thickness of the intrinsic layer contributes a lot to the process of generation of photogenerated carriers, which increases the performance of the solar cell. We have also observed that the increase in the density of the bulk defects of the intrinsic layer and the surface defects at the buffer layer/i-(a-Si:H) interface increases the recombination phenomena, which contribute to the reduction of a-Si:H-based solar cell performance. The optimized structure of the ultrathin a-Si:H-based solar cell gives a conversion efficiency of 12.71% for a thickness of $1\,\mu m$ and a bulk defect density of $10^9\,cm^{-3}$ of the intrinsic layer and a surface defect density of $10^{10}\,cm^{-2}$ at the buffer layer/i-(a-Si:H) interface.

Data Availability

All data used in our work has been cited in the reference list.

Conflicts of Interest

The authors declare that there is no conflict of interest regarding the publication of this paper.

Authors' Contributions

F. X. Abomo Abega performed the conceptualization, methodology, software use, and investigation and wrote the original draft. A. Teyou Ngoupo performed the conceptualization, methodology, software use, validation, and project administration and wrote the original draft. J.M.B. Ndjaka performed the conceptualization, methodology, supervision, and validation.

Acknowledgments

The authors acknowledge the use of SCAPS-1D software, developed by Marc Burgelman and colleagues at the University of Gent, in all the simulations reported in this paper.

References

[1] C. Case, N. Beaumont, and D. Kirk, "Industrial insights into perovskite photovoltaics," *ACS Energy Letters*, vol. 4, no. 11, pp. 2760–2762, 2019.

[2] L. Martini, L. Serenelli, F. Menchini, M. Izzi, and M. Tucci, "Silicon heterojunction solar cells toward higher fill factor," *Progress in Photovoltaics: Research and Applications*, vol. 28, no. 4, pp. 307–320, 2020.

[3] S. Banerjee, S. Mandal, S. Dhar, A. B. Roy, and N. Mukherjee, "Nanomirror-embedded back reflector layer (BRL) for advanced light management in thin silicon solar cells," *Industrial & Engineering Chemistry Research*, vol. 58, no. 28, pp. 12678–12686, 2019.

[4] S. Sriraman, S. Agarwal, E. S. Aydil, and D. Maroudas, "Mechanism of hydrogen-induced crystallization of amorphous silicon," *Nature*, vol. 418, no. 6893, pp. 62–65, 2002.

[5] J. É. Bourée and P. Roca i Cabarrocas, "Cellules solaires en couches minces à base de silicium," *Reflets de la physique*, no. 6, pp. 12–15, 2007.

[6] M. I. Kabir, S. A. Shahahmadi, V. Lim, S. Zaidi, K. Sopian, and N. Amin, "Amorphous silicon single-junction thin-film solar cell exceeding 10% efficiency by design optimization," *International Journal of Photoenergy*, vol. 2012, Article ID 460919, 7 pages, 2012.

[7] M. K. Hossain, "Hydrogenated amorphous silicon-based thin film solar cell: optical, electrical and structural properties," *Advanced Materials Research*, vol. 1116, pp. 59–64, 2015.

[8] M. A. Green, E. D. Dunlop, D. H. Levi, J. Hohl-Ebinger, M. Yoshita, and A. W. Ho-Baillie, "Solar cell efficiency tables (version 54)," *Progress in Photovoltaics: Research and Applications*, vol. 27, no. 7, pp. 565–575, 2019.

[9] C. Iliescu, B. Chen, D. P. Poenar, and Y. Y. Lee, "PECVD amorphous silicon carbide membranes for cell culturing," *Sensors and Actuators B: Chemical*, vol. 129, no. 1, pp. 404–411, 2008.

[10] X. Zhang, A. Cuevas, B. Demaurex, and S. De Wolf, "Sputtered hydrogenated amorphous silicon for silicon heterojunction solar cell fabrication," *Energy Procedia*, vol. 55, pp. 865–872, 2014.

[11] J. Plá, E. Centurioni, C. Summonte et al., "Homojunction and heterojunction silicon solar cells deposited by low temperature-high frequency plasma enhanced chemical vapour deposition," *Thin Solid Films*, vol. 405, no. 1-2, pp. 248–255, 2002.

[12] T. Shimizu, "Staebler-Wronski effect in hydrogenated amorphous silicon and related alloy films," *Japanese Journal of Applied Physics*, vol. 43, no. 6A, pp. 3257–3268, 2004.

[13] E. L. Salabaș, A. Salabaș, B. Mereu et al., "Record amorphous silicon single-junction photovoltaic module with 9.1% stabilized conversion efficiency on 1.43 m2," *Progress in Photovoltaics: Research and Applications*, vol. 24, no. 8, pp. 1068–1074, 2016.

[14] M. Stuckelberger, A. Billet, Y. Riesen et al., "Comparison of amorphous silicon absorber materials: kinetics of light-induced degradation," *Progress in Photovoltaics: Research and Applications*, vol. 24, no. 4, pp. 446–457, 2016.

[15] T. Pu, H. Shen, and Q. Tang, "Simulation of a charged Al_2O_3 film as an assisting passivation layer for a-Si passivated contact P-type silicon solar cells," *Silicon*, 2021.

[16] K. Decock, S. Khelifi, and M. Burgelman, "Modelling multivalent defects in thin film solar cells," *Thin Solid Films*, vol. 519, no. 21, pp. 7481–7484, 2011.

[17] M. Burgelman, K. Decock, A. Niemegeers, J. Verschraegen, and S. Degrave, *SCAPS Manual. Version: 23 January 2018*, 2018.

[18] B. P. Rand, J. Genoe, P. Heremans, and J. Poortmans, "Solar cells utilizing small molecular weight organic semiconductors,"

Progress in Photovoltaics: Research and Applications, vol. 15, no. 8, pp. 659–676, 2007.

[19] C. H. Hsu, X. Y. Zhang, H. J. Lin, S. Y. Lien, Y. S. Cho, and C. S. Ye, "Numerical simulation of crystalline silicon heterojunction solar cells with different p-type a-SiOx window layer," *Energies*, vol. 12, no. 13, p. 2541, 2019.

[20] J. Park, V. A. Dao, C. Shin et al., "A buffer-layer/a-SiO_x:H(p) window-layer optimization for thin film amorphous silicon based solar cells," *Thin Solid Films*, vol. 546, pp. 331–336, 2013.

[21] K. Hayashi, M. Kondo, A. Ishikawa, and H. Yamagisi, "ZnO-Ag sputtering deposition on a-Si solar cells," in *Proceedings of 1994 IEEE 1st World Conference on Photovoltaic Energy Conversion-WCPEC (A Joint Conference of PVSC, PVSEC and PSEC)*, pp. 674–677, Waikoloa, HI, USA, 1994.

[22] W. H. Kouider and A. Belfar, "Window layer thickness effect on amorphous silicon oxide solar cell performances," *Journal: Algerian Journal of Renewable Energy and Sustainable Development*, vol. 2, no. 1, pp. 67–74, 2020.

[23] N. Dwivedi, S. Kumar, S. Singh, and H. K. Malik, "Oxygen modified diamond-like carbon as window layer for amorphous silicon solar cells," *Solar Energy*, vol. 86, no. 1, pp. 220–230, 2012.

[24] P. Chelvanathan, M. I. Hossain, and N. Amin, "Performance analysis of copper-indium-gallium-diselenide (CIGS) solar cells with various buffer layers by SCAPS," *Current Applied Physics*, vol. 10, no. 3, pp. S387–S391, 2010.

[25] R. Lachaume, *Contribution à la caractérisation électrique et à la simulation numérique des cellules photovoltaïques silicium à hétérojonction, [Ph.D. thesis]*, Grenoble, 2014.

[26] S. De Wolf, A. Descoeudres, Z. C. Holman, and C. Ballif, "High-efficiency silicon heterojunction solar cells: a review," *Green*, vol. 2, no. 1, pp. 7–24, 2012.

[27] R. V. K. Chavali, J. R. Wilcox, B. Ray, J. L. Gray, and M. A. Alam, "Correlated nonideal effects of dark and light I–V characteristics in a-Si/c-Si heterojunction solar cells," *IEEE Journal of Photovoltaics*, vol. 4, no. 3, pp. 763–771, 2014.

[28] J. S. Park, S. Kim, Z. Xie, and A. Walsh, "Point defect engineering in thin-film solar cells," *Nature Reviews Materials*, vol. 3, no. 7, pp. 194–210, 2018.

[29] M. Rahmouni and S. Belarbi, "Defect pool numerical model in amorphous semiconductor device modeling program," *Journal of Nano-and Electronic Physics*, vol. 11, no. 2, pp. 02008-1–02008-5, 2019.

[30] T. Ouslimane, L. Et-Taya, L. Elmaimouni, and A. Benami, "Impact of absorber layer thickness, defect density, and operating temperature on the performance of $MAPbI_3$ solar cells based on ZnO electron transporting material," *Heliyon*, vol. 7, no. 3, article e06379, 2021.

[31] A. Ghahremani and A. E. Fathy, "High efficiency thin-film amorphous silicon solar cells," *Energy Science & Engineering*, vol. 4, no. 5, pp. 334–343, 2016.

[32] A. Teyou Ngoupo, S. Ouédraogo, and J. M. Ndjaka, "Numerical analysis of interface properties effects in CdTe/CdS:O thin film solar cell by SCAPS-1D," *Indian Journal of Physics*, vol. 93, no. 7, pp. 869–881, 2019.

[33] O. Astakhov, V. Smirnov, R. Carius et al., "Relationship between absorber layer defect density and performance of a-Si:H and μc-Si:H solar cells studied over a wide range of defect densities generated by 2 MeV electron bombardment," *Solar Energy Materials and Solar Cells*, vol. 129, pp. 17–31, 2014.

[34] G. M. Tcheum, A. T. Ngoupo, S. Ouédraogo, N. Guirdjebaye, and J. M. B. Ndjaka, "Numerical analysis of ultrathin Cu(In,Ga)Se2 solar cells with Zn(O,S) buffer layer," *Pramana*, vol. 94, no. 1, pp. 1–10, 2020.

[35] D. Rached and W. L. Rahal, "Investigation of the interface defect density at pm-Si:H/c-Si and the surface recombination speeds on silicon heterojunction solar cells," *Optik*, vol. 223, article 165575, 2020.

[36] B. Zhou, X. Yin, J. Zhang et al., "Numerical simulation of an innovative high efficiency solar cell with CdTe/Si composite absorption layer," *Optical Materials*, vol. 110, article 110505, 2020.